

1 **Geochemical evidence for intermediate water circulation in the westernmost**
2 **Mediterranean over the last 20 kyr BP and its impact on the Mediterranean outflow**

3 F.J. Jiménez-Espejo¹, M. Pardos-Gené², F. Martínez-Ruiz², A. García-Alix³, T. van de Flierdt⁴,
4 Takashi Toyofuku⁵, Andre Bahr⁶, Katharina Kreissig⁴.

5

6 ¹Department of Biogeochemistry, Japan Agency for Marine-Earth Science and
7 Technology(JAMSTEC), Yokosuka 237-0061, Japan

8 ² Instituto Andaluz de Ciencias de la Tierra (CSIC), Avenida de las Palmeras 4, 18100
9 Armilla (Granada), Spain

10 ³Department of Geographical and Earth Sciences, University of Glasgow, UK

11 ⁴Department of Earth Science and Engineering, Imperial College London, South Kensington
12 Campus, Prince Consort Road, London SW7 2AZ, UK

13 ⁵Department of Marine Biodiversity Research (Bio-dive), Japan Agency for Marine-Earth
14 Science and Technology(JAMSTEC), Yokosuka 237-0061, Japan

15 ⁶Institute of Earth Sciences, Heidelberg University, Heidelberg, Germany

16

17 fjspejo@jamstec.go.jp, mpardos@iact.ugr-csic.es, Antonio.Garcia-AlixDaroca@glasgow.ac.uk,
18 tina.vandeflierdt@imperial.ac.uk, toyofuku@jamstec.go.jp, andre.bahr@geow.uni-heidelberg.de,
19 k.kreissig@imperial.ac.uk

20

21 **Abstract**

22 The Mediterranean Outflow (MOW) is generated by deep and intermediate waters from
23 different basins in the Mediterranean Sea. Despite the number of studies on Mediterranean water
24 masses, little work has been done on the source and properties of intermediate waters in the
25 westernmost Mediterranean Sea and their links with MOW. Here we examine three marine
26 sediment records spanning the last 20 kyr, located at key depths to trace intermediate waters
27 along the Alboran Sea. We use a combination of redox-sensitive elements, which can serve as
28 proxies to reconstruct variations in the water column oxygenation and the Nd isotopic
29 composition of foraminiferal ferromanganese coatings, in order to reconstruct water mass
30 provenance of Eastern/Western Mediterranean waters.

31 As measured, $\epsilon_{Nd} < -9.2$ and a low U/Th ratio during glacial periods can be attributed to the
32 presence of Western Mediterranean Deep Water (WMDW) at the study sites. During deglaciation,
33 higher Nd isotopic compositions and U/Th ratios point to an enhanced contribution of
34 the modified Levantine Intermediate Water (LIW). The comparison between our data and other
35 LIW and MOW records suggests that i) the lower branch of MOW is linked to WMDW during the
36 glacial period, ii) the middle MOW branch follows LIW activity during deglaciation, while iii) the
37 upper branch is more active during late Holocene, coinciding with LIW formation increase after
38 sapropel deposits. This reconstruction has significant implications for an understanding of the
39 MOW evolution.

40

41

42 **1.Introduction**

43 The Mediterranean Sea is connected with the northeastern Atlantic Ocean through the
44 Strait of Gibraltar. The Mediterranean Outflow Water (MOW) has a strong impact on the
45 composition of North Atlantic intermediate waters, hence playing an important role in global
46 thermohaline circulation (Johnson, 1997; Sierro et al., 2005; Rogerson et al., 2006; Hernandez-
47 Molina et al., 2014; Ivanovic et al., 2014). A strong MOW input has been associated, for
48 example, with the recovery of the Atlantic thermohaline circulation after the Last Glacial
49 Maximum (e.g., Rogerson et al., 2006; Voelker et al., 2006). At present, the MOW is
50 predominantly fed by intermediate and deep Mediterranean waters (Bryden and Stommel, 1984).

51 A key location for understanding MOW is the Alboran Sea, within the westernmost
52 Mediterranean. Most previous studies involving the Alboran Sea (e.g., Barcena et al., 2001;
53 Cacho et al., 2001; Martrat et al., 2004; Moreno et al., 2005; Jimenez-Espejo et al., 2007; Rohling
54 et al., 2015 and references therein) focus on reconstructing surface water and deep water
55 conditions, while information about intermediate waters remains scarce. Yet compared to surface
56 and deep water masses, intermediate waters display distinct hydrographic features (e.g. Font,
57 1987; Millot, 2009), and a very characteristic geochemical fingerprint (e.g. their Nd isotopic
58 composition; Tachikawa et al., 2004).

59 A key open question is how to reconstruct the source and properties of Mediterranean
60 intermediate waters and their relationship with the MOW. In studying relative water mass
61 contributions to the MOW during the last deglaciation and the Holocene, we deploy a range of
62 geochemical proxies on three sediment records recovered in the Alboran Sea basin. The cores are
63 located at depths between 1800 and 2400 mbsf, allowing for an intermediate/deep water mass

64 reconstruction (De Lange et al., 2008, Tachikawa et al., 2015). The utilized proxies include the
65 Nd isotopic composition of seawater as a quasi-conservative water mass proxy, as well as redox
66 sensitive trace elements to constrain the redox conditions in the water column. Our new data may
67 provide novel insights into the evolution of Levantine Intermediate Water (LIW) and
68 Mediterranean thermohaline circulation, leading to an improved understanding of the MOW over
69 time.

70

71 **Oceanographic setting**

72 The general circulation in the Mediterranean is a result of high evaporation rates and
73 MOW activity (Ovchinnikov et al., 1976; Millot et al., 2009; MerMEX group, 2011). In the
74 Western Mediterranean Sea (WMS), three main water masses can be distinguished: Modified
75 Atlantic Water (MAW), Levantine Intermediate Water (LIW), and Western Mediterranean Deep
76 Water (WMDW). The MAW forms as a result of the comparatively fresh Atlantic water ($S < 36.5$)
77 entering the Mediterranean Sea via the strait of Gibraltar and mixing with the surface waters of
78 the Alboran Sea. The MAW flows eastward as a 150-200 m thick surface layer.

79 On the other hand, the LIW originates in the Eastern Mediterranean Sea (EMS) through
80 sinking during winter times (Cramp and O'Sullivan, 1999) and can be identified in the study area
81 at depths between 200 and 600 m. Finally, WMDW is found below this water depth, being
82 generated by surface cooling in the Gulf of Lion. Its main flow path is along the Moroccan
83 margin (Hernandez-Molina et al., 2002).

84 The MOW comprises a mixture of these deep and intermediate water masses (Parrilla et
85 al., 1986; Millot et al., 1999) (Figs. 1 and 2). Its formation has been related to the wind strength,

86 predominant circulation patterns of source waters, freshwater input, temperatures and the density
87 of surface waters, among other factors (e.g., Rohling and Bryden, 1992; Bethoux et al., 1998;
88 Cramp and O'Sullivan, 1999; Millot, 2009).

89

90 **2. Materials and methods**

91 **2.1. Site description and age model**

92

93 We obtained our data from Sites 300G, 302G and 304G, situated at different depths
94 (1860m, 1989m, and 2382m, respectively; Table 1) along the west-east trending East Alboran
95 basin slope; they are currently bathed in the WMDW (Figs. 1 and 2). The incoming MAW flow
96 generates a quasi-permanent anticyclonic gyre in the western Alboran Sea and a transient gyre at
97 the eastern part of the basin (Fig. 1). The hydrological front is characterized by a strong
98 horizontal density gradient ($>0.4 \text{ kg m}^{-3}$) between MAW and the LIW (Tolosa et al., 2003).

99 Age models for the three sites have been published previously (Jimenez-Espejo et al.,
100 2008) and are based on monospecific planktonic foraminifera ^{14}C -AMS dates (accelerator mass
101 spectrometry), stable isotope stratigraphy, and the correlation of geochemical elemental ratio
102 profiles among sites. The cores span the past 20 kyr BP (Table 1) and were collected during
103 Training-Through-Research (TTR) Cruise 14 in order to track shifts in the water column
104 structure. Recovered lithologies comprise homogenous greyish olive nannofossil clay and
105 nannofossil-rich silty clay (Comas and Ivanov, 2006). The studied intervals and their detrital
106 elemental composition show no indication of grain-sorting processes, indicative of strong bottom
107 currents, or turbiditic sequences (Jimenez-Espejo et al., 2008). Sedimentation rates in the Alboran
108 basins range from approximately 10 cm/ka during the late Holocene up to 20 cm/kyr during some

109 pre-Holocene periods. Sampling resolution was 3 cm at site 300G and between 3 and 7 cm at sites
110 302 and 304, yielding a temporal resolution of ~200 to ~500 yrs depending on site and time interval.

111

112 **2.2. Methods**

113 Major element concentrations (Fig. 3) were obtained by atomic absorption spectrometry
114 (AAS) (Perkin-Elmer 5100 spectrometer), with an analytical error of 2%, at the Instituto Andaluz
115 de Ciencias de la Tierra (CSIC-UGR). Analysis of trace elements (U, Th and Ba) was performed
116 using inductively coupled plasma-mass spectrometry (Perkin-Elmer Sciex Elan 5000 ICP-MS)
117 following HNO₃ + HF digestion. Measurements were carried out as triplicates using Re and Rh
118 as internal standards at the Centro de Instrumentación Científica (University of Granada).
119 External reproducibility was determined by dissolving 10 replicates of powdered samples and
120 results were in agreement within 3% for analyte concentrations of 50 ppm and within 8% for
121 analyte concentrations of 5 ppm (Bea, 1996). From the suite of analyzed major and trace elements,
122 U, Th and Ba (and corresponding normalized concentrations) were selected as proxies for water
123 mass reconstructions.

124 Authigenic Nd isotopic compositions of bottom waters were reconstructed based on the Fe-
125 Mn oxide coatings around foraminifera tests in the MAGIC laboratories at Imperial College,
126 London, following the pioneering work of Roberts et al. (2010) (Table 2). Briefly, ~80 mg of
127 planktonic foraminifera were picked from the >125 μm fraction of 11 sediment samples from two
128 different coresites (304G and 302G) located in the western gyre of the Alboran Sea. Sampled
129 tests were crushed between glass plates, ensuring that all chambers were opened. Thereafter,
130 samples were ultrasonicated in glass beakers (with 5 ml de-ionized water) for ~1 minute before

131 pipetting off the waste water. This step was repeated until the water was clear (i.e., no clay left).
132 The cleanliness of samples was checked under a microscope and visible pieces of pyrite and
133 detrital particles were removed. Digestion of foraminifera was achieved by addition of 1ml of 1M
134 acetic acid.

135 Additionally, four samples from sites 302G and 304G were investigated for their detrital
136 Nd isotopic composition following sequential extraction of authigenic carbonate and
137 ferromanganese coatings as described previously (see Biscaye, 1965, and Rutberg et al., 2000)
138 (Table 2). ~50mg of detrital material was digested on a hotplate using a mixture of 0.5ml 20M
139 HClO₄, 1ml 15M HNO₃ and 3ml 27M HF. After conversion to nitrate form, Nd was separated
140 from the sample matrix and other rare earth elements by means of two-step ion chromatography
141 (TRU-spec and Ln-spec columns; modified after Pin and Zalduegui, 1997). Neodymium isotope
142 measurements were carried out on a Nu Plasma-HR MC-ICPMS. Instrumental mass bias was
143 corrected for using a ¹⁴⁶Nd/¹⁴⁴Nd ratio of 0.7219 and an exponential law. Samarium interferences
144 were monitored and were significantly below the correctable level of 0.1% ¹⁴⁴Sm on ¹⁴⁴N in all
145 samples. Repeated analyses of the JNdi-1 standard yielded values of 0.512107 ± 0.000014,
146 0.512133 ± 0.000015, 0.512121 ± 0.000014, and 0.512072 ± 0.000011 (2sd) over the course of
147 the four days of sample analyses. All sample results are reported relative to a JNdi-1 ¹⁴³Nd/¹⁴⁴Nd
148 value of 0.512115 (Tanaka et al., 2000).

149

150 **3. Paleoenvironmental proxies**

151 **3.1. Neodymium isotopes as water mass proxies**

152 Neodymium isotope ratios in seawater are often used in paleoceanography as a quasi-
153 conservative tracer of water masses (e.g., Frank et al., 2002; Goldstein and Hemming, 2003).
154 Neodymium isotopes are expressed as ϵ_{Nd} and denote the deviation of a measured $^{143}Nd/^{144}Nd$
155 ratio from the Chondritic Uniform Reservoir (CHUR) in parts per 10,000 (present day CHUR =
156 0.512638; Jacobsen and Wasserburg, 1980). Geological heterogeneity in the continents and their
157 subsequent erosion and delivery to the ocean, as well as exchange of seawater with the ocean
158 margins, leave distinct Nd imprints on water masses, which can be traced spatially due to the
159 short residence time of Nd in the seawater (~400 years; Tachikawa et al., 2003). Modern
160 seawater Nd isotopic compositions range from values as low as $\epsilon_{Nd} < -20$ in the Labrador Sea,
161 which is surrounded by old continental crust, to values as high as $\epsilon_{Nd} \sim 0$ in the North Pacific,
162 close to young volcanic inputs (see Lacan et al., 2012, and Jeandel et al., 2007 for an overview).
163 The origin and significance of ϵ_{Nd} in the Mediterranean Sea has been previously explored,
164 indicating that LIW has an isotopic signature of $\epsilon_{Nd} \sim -5$ in the EMS (Tachikawa et al., 2004;
165 Vance et al., 2004). However, this value becomes less radiogenic in the WMS, where ϵ_{Nd} values
166 of ~ -8.9 are observed at LIW depths (Henry et al., 1994; Tachikawa et al., 2004). LIW reaches
167 these values after crossing the strait of Sicily. Hereafter we will refer to this signature at
168 intermediate depths in the WMS as modified LIW (mLIW). Less radiogenic values are
169 characteristic of WMDW ($\epsilon_{Nd} = -9.4$; Henry et al., 1994; Tachikawa et al., 2004), the least
170 radiogenic values being recorded in MAW ($\epsilon_{Nd} = \sim -10.4$; Spivack and Wasserburg, 1988;
171 Tachikawa et al., 2004) (Fig. 3). When interpreting the Nd isotopic composition of seawater as
172 derived from authigenic phases in sediments, it should be noted that intense sediment reworking
173 and along-slope transport may alter the use of Nd isotopes as a water mass proxy (e.g., Gutjahr et
174 al., 2008). The Gulf of Cadiz is one such area (Stumpf et al. 2010), though contourites are not

175 described in the eastern Alboran region (Palomino et al., 2011); hence we are confident that Nd
176 isotopes can reliably trace water masses.

177

178 **3.2. U as paleoceanographic proxy**

179 Uranium in sediments can be hosted in solid phases such as detrital lithogenic
180 components (physically transported to and deposited at the site), in authigenic phases (associated
181 with biogenic carbonate and organic biomass), or be derived from reductive authigenic pore-
182 water precipitation (Andersen et al., 2014).

183 Because U concentrations in the sediment might be further biased by detrital input, the
184 U/Th ratios used. Normalization of trace element contents to an immobile element—usually Al
185 or Th—is common in paleoceanographical studies, and a vast literature on geochemical proxies
186 demonstrates the usefulness of this ratio (e.g., Van der Weijden, 2002; Calvert and Pedersen,
187 2007). In this sense, the U/Th ratio allows for correcting the dilution by sedimentary phases
188 barren of a particular trace element. The U/Th ratio thus represents the excess of U with respect
189 to Th (aluminosilicate fraction). The subtraction of the detrital influence on trace elements
190 concentrations is an important issue discussed by different authors (e.g., Chase et al., 2001;
191 Tribouillard et al., 2006; Andersen et al., 2014). Hence, it is important to distinguish whether
192 uranium enrichment is linked to bottom water oxygenation and/or organic matter oxidation and
193 consequent post-depositional sediment reduction forcing U deposition from pore waters (when
194 pore-water nitrate vanishes in sediments beneath the redoxcline, U^{+6} is reduced to immobile U^{+4}
195 and precipitates; Anderson, 1982; Barnes and Cochran, 1990; Mangini et al., 2001). Although
196 the specific behavior of U under oxic and suboxic conditions remains poorly understood, an

197 increase in U deposition has been observed in suboxic basins with respect to oxidized
198 conditions (Andersen et al., 2014). In the WMS, the last organic rich layer (ORL 1, between 14.5
199 and 8.2 ka) has been associated with the occurrence of sluggish bottom waters (Rogerson et al.,
200 2006). U/Th enrichment is observed for sediments deposited during this ORL interval, and
201 partially the GS-2a period, when Ba based proxies also support enhanced productivity (Fig. 3e).
202 Consequently, the WMS U/Th ratio appears to be predominantly sensitive to suboxic
203 conditions at the sea floor, and furthermore correlates with organic matter deposition.

204

205 **4. Results**

206 Major element concentrations in 355 samples were obtained by AAS; 360 samples were
207 analyzed using inductively coupled plasma-mass spectrometry. Nd isotopic composition was
208 determined in 15 samples, 11 in the authigenic Fe-Mn oxide coatings around foraminifera tests
209 and 4 in bulk samples (Table 2). All datasets are unpublished to date, except the Barium excess
210 content during the 20 to 5 kyr interval, previously discussed in Jimenez-Espejo et al., 2008.

211 U content ranged between 1 and 5 ppm, showing the lowest values at site 304G during
212 late Holocene. Higher values are associated to the deglaciation period ($U > 3$ ppm), whereas
213 lower values can be found during the last Glacial maximum and after 8.0 kyr. The content varies
214 between 5 and 9 ppm, the highest values reached during late Holocene at site 302G.

215 The Ba content derived from marine barite (Ba excess) was obtained by subtracting the
216 amount of terrigenous Ba from the total Ba content (Dymond et al., 1992; Eagle et al., 2003).
217 The presence of marine barite was confirmed by Field Emission Scanning Electron
218 Microscopy (FESEM). Barite crystals were found with sizes and morphologies corresponding to

219 typical marine barite(1-5 mm in size, with round and elliptical crystals). Ba excess is calculated
220 as: $Ba\ excess = (Ba\text{-total}) - Al\ (Ba/Al)_c$, where Ba-total and Al are concentrations in ppm, and
221 $(Ba/Al)_c$ is the crustal ratio for these elements. In this study, we used the value $(Ba/Al)_c = 0.033$,
222 as estimated by Sanchez-Vidal et al., 2005 in the Alboran basin. During the last 5 ka interval all
223 studied sites show a nearly parallel and flat pattern, having Ba excess values around 250 ppm
224 (Fig. 3e).

225 In turn, the ϵ_{Nd} values obtained for the authigenic fraction range from $\epsilon_{Nd} -10.1 \pm 0.3$ for
226 the deepest site (304G) during the last glacial period, to $\epsilon_{Nd} -9.09 \pm 0.28$ for the shallowest site
227 (302G) during late Holocene. Measured ϵ_{Nd} values in bulk samples are clearly different from the
228 authigenic ones, with ϵ_{Nd} values between -12.62 ± 0.28 and -12.82 ± 0.28 (Table 2).

229

230 **5. Discussion**

231 **5.1. Last Glacial Maximum and deglaciation**

232 During the last glacial maximum, a low sea level combined with cold and arid conditions
233 over the Gulf of Lion (Hayes et al., 2005) have been associated with intense deep water formation
234 in the WMS (Rogerson et al., 2008). Around 19.8 ka cal BP we obtained a ϵ_{Nd} value of $-9.6 \pm$
235 0.29 for site 302G and $\epsilon_{Nd} -10.1 \pm 0.3$ for site 304G (Fig. 3b), values typically associated with
236 modern water masses generated in the Gulf of Lion (Henry et al., 1994; Tachikawa et al., 2004)
237 (Fig. 3b). At all our studied sites U/Th ratios show relatively low values, between 0.25 and 0.4,
238 suggesting well ventilated water mass generated in the WMS. For the same time period,
239 Toucanne et al. (2012) described an intense LIW flow at the Corsica Trough (MD01-2434; Fig.

240 3d). Furthermore, a dense MOW, flowing at deeper depths than today, has been reconstructed in
241 the Gulf of Cadiz (Rogerson et al., 2005; Voelker et al., 2006; Llave et al., 2007), with low
242 activity in the upper MOW branch (Bahr et al., 2014). We therefore conclude that
243 WMDW predominance in the Alboran basin is coincident with enhanced activity of the deeper
244 MOW branch during the last glacial maximum. The probable causes of this relationship will be
245 discussed in more detail below.

246 Environmental conditions in the Alboran Sea appear to change around 18 ka cal BP,
247 contemporaneous with progressive deglaciation affecting atmospheric CO₂ and methane contents
248 (e.g., Marcott et al., 2014), as well as the Atlantic meridional circulation (McManus et al.,
249 2004). Our Nd records indicate a shift from values around -10.1 ± 0.3 during the glacial period, to
250 less radiogenic ones reaching $\epsilon_{Nd} = -9.0 \pm 0.3$ at site 302G at 15.8 ka cal BP (Fig. 3b). Such
251 higher values are typically associated with water masses generated in the EMS (Henry et al.,
252 1994; Tachikawa et al., 2004). Furthermore, from 17.5 ka cal BP onward U/Th ratios increase at all
253 sites, with a subtle difference among them (Fig. 3 dashed line). At the shallower sites, 300G and
254 302G, oxygenation decreases before the same trend is observed at the deeper site 304G, pointing
255 to a depth-dependent bottom and/or pore waters ventilation. Despite the dating uncertainties,
256 similar depth-dependent ventilation variations have been invoked in the EMS basins related to
257 sapropel S1 deposition (De Lange et al., 2008; Tachikawa et al., 2015). These changes can be
258 explained by progressive water mass mixing or replacement of WMS-generated deep waters,
259 and/or by deepening of EMS-generated intermediate waters (LIW) from 1,900 and 2,300 mbsf. It
260 is noteworthy that we observe a peak in LIW intensity in the Corsica site (Toucanne et al., 2012;
261 Fig. 3d) at the same time when the LIW influence appears to affect the shallowest sites in the
262 Alboran Sea. This decrease in the WMDW contribution to the MOW should have increased the

263 MOW buoyancy and decreased the flux in the lower core of the MOW, as can be interpreted
264 from the records in the Gulf of Cadiz (Voelker et al., 2006). Nevertheless, no changes are
265 observed in the MOW upper branch (Fig. 3c) (Bahr et al., 2014). Hence, changes in water masses
266 within the Alboran region can be tracked in the Gulf of Cadiz, in this case a mLIW
267 intensification that is connected to a ceased MOW lower core.

268 The next change in environmental conditions that is recorded in the Alboran region took
269 place during the GS-1 (Younger Dryas, YD) (Fig. 3). Ba/Al and U/Th ratios show an
270 increase during the YD at the deepest site (304G), pointing to lower oxygenation and higher
271 productivity, which coincides with the maximum intensity of LIW flow in the central
272 Mediterranean Sea (Fig. 3d) (Toucanne et al., 2012). This increase in marine productivity is also
273 documented by the diatom record from Alboran basin (Barcena et al., 2001). In the Gulf of Cadiz
274 (Site U1387; Bahr et al., 2014), a concomitant reactivation of the upper branch of MOW, as
275 reconstructed from Zr/Al ratios, indicates higher MOW buoyancy during this period (Fig. 3c). A
276 weak contribution of the WMDW to the MOW is fostered by the Nd data that point to a persistent
277 influence of the LIW waters at site 302G (Fig. 3b). Furthermore, the studied proxies indicate that
278 the cooling associated with the YD did not lead to a significant reactivation of WMDW
279 formation. This observed low oxygenation in the WMS during the YD seems to contradict model
280 results that predict high ventilation during this period (Rogerson et al., 2012a). Our data therefore
281 reveal a marked difference between the EMS, with intense thermohaline circulation, and the
282 WMS, with sluggish circulation during the YD. It appears that the Eastern Mediterranean Basin
283 was more prone to alterations in the water mass structure than the western basin (Sprovieri et al.,
284 2002; Hayes et al., 2005; Hennekam et al., 2014).

285

286 5.2 Holocene and sapropel deposition

287 During the Holocene, the Eastern and Western Mediterranean Basins show
288 distinct signatures. In the Eastern basin, a characteristic feature was the deposition of the most
289 recent sapropel (S1), an organic-rich black layer, deposited between 10.8 ± 0.4 and 6.1 ± 0.5 kcal
290 BP (Ariztegui et al., 2000; De Lange et al., 2008). However, no such deposits can be found in the
291 WMS, where the last ORL formed between 14.5 and 8.2 ka (Cacho et al., 2002; Rogerson et al.,
292 2008; Rohling et al., 2015).

293 During the early/middle Holocene (until 8.2 ka BP), the studied records display high
294 U/Th ratio values (around 0.6), indicating a relatively low oxygenation in agreement with the
295 S1a deposition (Fig. 3a). The Nd isotopic composition of seawater around 6.8 ka cal BP at site
296 302G ($\epsilon_{Nd} - 9.75 \pm 0.27$) shows values similar to those related with WMDW formation during the
297 Last Glacial Maximum, pointing to a WMDW reactivation—or at least a LIW reduction—while
298 sapropel S1 deposition was still active. Weak LIW formation has also been described in the EMS
299 during sapropel deposition and has been linked with increase runoff and fluvial input from the
300 Nile (Bosmans et al., 2015; Rohling et al., 2015).

301 During the late Holocene, more radiogenic Nd isotope values indicate a mLIW influence
302 (Fig. 3b). This recovery of the EMS signal is coincident with a progressive increase in the MOW
303 upper branch (Fig. 3c). Notably, the central Mediterranean LIW record (Fig. 3d) does not show
304 any variations associated with the sapropel demise, nor does it reveal any significant changes
305 throughout the entire Holocene. Previous work has described an antiphased pattern between the
306 EMS and the WMS in the late Holocene (Rimbu et al., 2004; Roberts et al., 2008; Felis and
307 Rimbu, 2010; Martín-Puertas et al., 2010), with humid conditions in the WMS (Martín-Puertas et

308 al., 2010) but dry conditions in the EMS (e.g., Nieto-Moreno et al., 2013). These differences
309 between basins can be related to the W-E gradients in salinity and temperature, different
310 influences of riverine input, and diverging climate patterns especially during winter (e.g., Hayes
311 et al., 2005).

312 Overall, observed variations during the Holocene indicate a high sensitivity of the
313 Mediterranean thermohaline circulation to fresh water input. In detail, model results indicate that
314 as little as 5%-10% changes in the Mediterranean mean freshwater budget may have pronounced
315 effects on the overturning circulation in the area (Skirris et al., 2007).

316

317 **5.3. Origin and significance of simultaneous changes recorded between records from the** 318 **Alboran Sea and MOW**

319 Comparison between our records from the Alboran sites and previously published
320 MOW records indicates a complex regional picture. Despite the fact that the WMS thermohaline
321 circulation is affected by a number of factors throughout time —such as interaction between sea-
322 level rise, meltwater pulses, monsoon flooding, Gibraltar strait section and Alpine melt-water
323 routing (e.g., Rohling et al., 2015)—our new data reveal some insightful patterns. In detail, our
324 observations indicate that (i) the MOW's lower branch is linked to the WMDW evolution, (ii) its
325 middle branch follows the LIW activity, and (iii) its upper branch is more active during times of
326 minima in WMDW formation. This marked heterogeneity of the MOW is in agreement with
327 present day oceanographic observations of different Mediterranean waters in the Gibraltar
328 strait (Naranjo et al., 2012; Millot et al., 2014) and three distinct MOW branches (e.g., Ambar et
329 al., 2002).

330 The described correlations between the two water masses can be causal or genetic. A
331 causal relation would have major consequences for understanding the MOW behavior, because
332 the WMDW, formed in the Gulf of Lion, is mainly driven by the North Atlantic climate realm
333 (Cacho et al., 2002; Frigola et al., 2007). In contrast, the LIW is mainly affected by the Eastern
334 Mediterranean realm and conditioned by variations in high and low latitude climates (e.g.,
335 Blanchet et al., 2013; Hennekan et al., 2014). If causal, the main mechanisms driving the MOW
336 branch intensification could be freshening of the Mediterranean Sea surface, thereby influencing
337 bottom water formation (MerMex group, 2011). Enhanced fresh water input has been related to
338 Nile run-off (Rossignol-Strick et al., 1982; Rohling, 1994; Rohling et al., 2015), meltwater
339 fluxes (Ehrmann et al., 2007), and Black Sea influence (Grimm et al., 2015). Climate models
340 indicate that precipitation patterns as well as runoff from the Nile are driven by the strength of the
341 North African monsoon, ultimately responding to northern hemisphere summer
342 insolation (Bosmans et al., 2015). In such a scenario, water mass variations at the studied core
343 sites can be interpreted to manifest the influence of surface processes on deep sea circulation in
344 the Mediterranean.

345 Nonetheless, hydrodynamic models reject a causal link between downwelling in the
346 Mediterranean and MOW evolution, and instead propose sea-level variability and water column
347 density in the Eastern Atlantic as main driving factors for MOW deepening and branch activity
348 (Rogerson et al., 2012a;b). In this case, the described correlation between both sides of the
349 Gibraltar strait water masses could be linked genetically, through common climate and
350 environmental variations. More specifically, the water column density gradient in the Gulf of
351 Cadiz would have increased during deglaciation due to the production of meltwater from ice
352 sheets and glaciers (Rogerson et al., 2012b). This gradient increase would in turn promote a

353 MOW shoaling due to the presence of dense Atlantic water masses at shallower depths and
354 surface freshening in the Mediterranean, leading to reduced WMDW formation at the same
355 time. This genetic link is, however, difficult to reconcile with observed changes during the late
356 Holocene, a period of almost stable sea level.

357 No matter which of the two mechanisms is preferred, our data certainly point to an
358 intrinsic correlation between Mediterranean intermediate water masses and MOW branches.
359 Deciphering this correlation in more detail calls for a targeted study of geochemical proxies in all
360 three MOW branches (lower, middle, and upper) to discern whether they preserve an EMS or
361 WMS climate realm signal. Based on the results presented here, we can speculate that the middle
362 and upper branch were probably dominated by low latitude climate variations, whereas the lower
363 branch would be more sensitive to a higher latitudinal signal.

364

365 **6. Conclusions**

366 Geochemical proxies provide evidence of significant paleoceanographic changes in the
367 western Mediterranean during the last 20 ka BP. We observe a replacement (or reduced
368 influence) of relatively cold and well oxygenated bottom waters generated in the WMS during
369 GS-2a by less oxygenated intermediate water masses of Eastern Mediterranean provenance in
370 key depth locations. The Eastern water mass appears to have influenced shallower water depths
371 in the Alboran Sea during the entire deglaciation and until the early Holocene.

372 Comparison of the Alboran records with previously published records of LIW intensity
373 from the Central Mediterranean, as well as MOW intensity in the Gulf of Cadiz, suggests a
374 heterogeneous MOW linked to Mediterranean intermediate water variations. The lower

375 branch seems to be mainly fed by the WMDW, while the middle and upper branch would
376 be linked to LIW activity. Nevertheless, we cannot determine whether the described
377 relationships are causally or genetically based. Placing our results into the context of Northern
378 Hemisphere climate variations, the lower branch of MOW is apparently dominated by high
379 latitude climate variations, and the middle and upper branches are instead forced by low latitude
380 evolution. More detailed studies are needed to fully resolve what drives changes in the different
381 branches of MOW over time, and how they are associated with regional and global climate
382 changes.

383

384 **Acknowledgements**

385 The authors are indebted to Dr. Zhengtang Guo as editor, Dr. M. Rogerson and two
386 anonymous reviewers for their invaluable comments and reviews. This study was supported by the
387 European Regional Development Fund (ERDF)-financed grants CGL2009-07603 and CGL2012-
388 32659 (Secretaría de Estado de Investigación MINECO), Project RNM 5212 and Research
389 Group RNM 179 (Junta de Andalucía). We are grateful to the Training-Through-Research
390 Programme for providing the core sediments analyzed. We acknowledge the Centre for
391 Scientific Instrumentation (CIC-University of Granada), the Poznan Radiocarbon Laboratory
392 (Poland), Andalusian Institute of Earth Sciences (IACT, CSIC-UGR), Department of Mineralogy
393 and Petrology (UGR) and Imperial College (U.K.) for analytical facilities. We also thank D.
394 Ortega and E. Holanda, C. Niembro, L. González, E. Abarca and J. Santamarina, as well as the
395 CIC personnel for their laboratory assistance. T.T. measurements are supported by grants-in-aid
396 for scientific research by MEXT/JSPS (2074031 and 25247085 to T.T.).

397

398 **Table and Figure captions**

399 **Figure 1.** a) Map of the western Mediterranean Sea with setting of studied gravity cores
400 300G, 302G and 304G in the Alboran Sea. Also shown are sites IODP-U1387 and MD01-2434
401 for comparison. Black and dashed gray lines represent the flow directions of major water masses,
402 Western Mediterranean Deep Water (WMDW), Levantine Intermediate Water (LIW) and
403 Modified Atlantic Water (MAW). b) Cross-section showing water mass stratification in the
404 Mediterranean. Modified from Cramp and O'Sullivan (1999).

405 **Figure 2.** Gibraltar Strait and Alboran basin bathymetry and raised-relief maps with
406 vertically exaggerated scale viewed from the East. Dashed lines represent the pathways of the
407 main currents in the area (modified from Hernandez-Molina et al., 2002). Modified Atlantic
408 Water (dark blue), Levantine Intermediate Water (green), and Western Mediterranean Deep
409 Water (light blue). Red line represents the coast line.

410 **Figure 3.** Time series of geochemical proxies for studied sites TTR-300G, TTR-302G, and
411 TTR-304G from the Alboran Sea (this study) in comparison to previously published records
412 from the area. a) U/Th ratios for sites 300G (red), 302G (blue) and 304G (orange), used as a
413 proxy for the degree of anoxia. b) Neodymium isotope composition of planktonic foraminifera
414 ferromanganese coatings at sites 302G and 304G used as a water mass provenance indicator.
415 Green and blue dark bands respectively display the main range of seawater Nd isotopic
416 composition of modified Levantine Intermediate Water (mLIW) ($\epsilon\text{Nd} \sim -8.9$, Tachikawa et al.,
417 2004) and the West Mediterranean Deep Water (WMDW) ($\epsilon\text{Nd} \sim -9.4$, Tachikawa et al., 2004).
418 Extended light green and blue bands denote full values range. c) Ln Zr/Al ratio at site U1387

419 (Gulf of Cadiz), an upper MOW intensity proxy (Bahr et al., 2014). d) Sortable Silt content at
420 site MD01-2434, an LIW intensity proxy (Toucanne et al., 2012). e) Barium excess (ppm) age
421 plotted comparison among cores (Jimenez-Espejo et al., 2008). Light blue bars across the Figure
422 indicate the African Humid Period and the last Organic Rich Layer (ORL) deposited in the
423 Western Mediterranean. Light grey bars indicate Greenland Stadials 2a, Sapropel S1a and S1b
424 (Ariztegui et al., 2000).

425

426 **Table 1.** Core data including location, water depth, studied interval and linear sedimentation rates.

427

428 **Table 2.** Nd isotopic compositions of foraminiferal coatings and bulk sediments from studied
429 sites. (a) Measured Nd isotopic composition normalized to JNdi $^{143}\text{Nd}/^{144}\text{Nd}$ value of 0.512115
430 (Tanaka et al., 2000). JNdi results for the four measurement sessions are reported in the main
431 text. (b) Internal 2σ standard error of the measurements. (c) ϵNd values are calculated relative to
432 a CHUR value of 0.512638 (Jacobsen and Wasserburg, 1980). (d) External errors are the 2σ
433 deviations derived from repeat analysis of the JNdi standard during the measurement sessions at
434 similar concentrations to sample sizes (10-20 ng Nd). Uncertainties plotted in Figure 3 are
435 internal 2σ standard errors.

436

437

438

439

440 **References**

441

442 Ambar, I., Serra, A., Brogueira, M.J., Cabeçadas, G., Abrantes, F., Freitas, P., Gonçalves, C. and
443 Gonzalez, N., 2002. Physical, chemical and sedimentological aspects of the Mediterranean
444 outflow off Iberia. *Deep Sea Res Part II*, 49, 4163-4177.

445 Andersen, M.B., Romaniello, S., Vance, V., Little, S.H., Herdman, R. and Lyons, T.W., 2014. A
446 modern framework for the interpretation of $^{238}\text{U}/^{235}\text{U}$ in studies of ancient ocean redox. *Earth
447 Planet Sci Lett*, 400, 184-194.

448 Anderson, R.F., 1982. Concentration, vertical flux and remineralization of particulate uranium in
449 seawater. *Geochim Cosmochim Acta*, 46, 1293-1299.

450 Ariztegui, A., Asioli, J.J., Lowe, F., Trincardi, L., Vigliotti, F., Tamburini, C., Chondrogianni,
451 C.A., Accorsi, M., Bandini Mazzanti, A.M., Mercuri, S., Van der Kaars, J.A. and McKenzie, J.,
452 2000. Palaeoclimate and the formation of sapropel S1: Inferences from Late Quaternary
453 lacustrine and marine sequences in the central Mediterranean region. *Palaeogeogr Palaeocl*,
454 158(3), 215-240, doi: 10.1016/S0031-0182(00)00051-1.

455 Bahr, A., Jiménez-Espejo, F.J., Kolasinac, N., Grunert, P., Hernández-Molina, F.J., Röhl, U.,
456 Voelker, A.H.L., Escutia, C., Stow, D.A.V., Alvarez-Zarikian, C.A. and Hodell, D.A., 2014.
457 Deciphering bottom current strength and paleoclimate signals from contourite deposits in the
458 Gulf of Cádiz during the last 140 ka: an inorganic geochemical approach. *Geochem Geophys
459 Geosy*, 15(8), 3145-3160, doi:10.1002/2014GC005356.

460 Barcena, M.A., Cacho, I., Abrantes, F., Sierro, F.J., Grimalt, J.O. and Flores, J.A., 2001.
461 Paleoproductivity variations related to climatic conditions in the Alboran Sea (western
462 Mediterranean) during the last glacial–interglacial transition: the diatom record. *Palaeogeogr
463 Palaeocl*, 167, 337-357.

464 Barnes, C.E. and Cochran, J.K., 1990. Uranium removal in oceanic sediments and the oceanic U
465 balance. *Earth Planet Sci Lett*, 97, 94-101.

466 Bea, F., 1996. Residence of REE, Y, Th and U in granites and crustal protoliths; implications for
467 the chemistry of crustal melts. *J Petrol*, 37, 521-552, doi:10.1093/petrology/ 37.3.521.

468 Bethoux, J.P., Morin, P., Chaumery, C., Connan, O., Gentili, B. and Ruiz Pino, D., 1998.
469 Nutrients in the Mediterranean Sea, mass balance and statistical analysis of concentrations with
470 respect to environmental change. *Mar Chem*, 63, 155-169, doi:10.1016/S0304-4203(98)00059-0.

471 Biscaye, P.E., 1965. Mineralogy and sedimentation of recent deep-sea clay in the Atlantic Ocean
472 and adjacent seas and oceans. *Geol Soc Am Bull*, 76, 803-831.

473 Blanchet, C.L., Tjallingii, R., Frank, M., Lorenzen, J., Reitz, A., Brown, K., Feseker, T. and
474 Brückmann, W., 2013. High- and low-latitude forcing of the Nile River regime during the
475 Holocene inferred from laminated sediments of the Nile deep-sea fan. *Earth Planet Sci Let*, 364,
476 98-110.

477 Bosmans, J.H.C., Drijfhout, S.S., Tuenter, E., Hilgen, F.J. and Lourens, L.J., 2015. Response of
478 the North African summer monsoon to precession and obliquity forcings in the EC-Earth GCM.
479 *Clim Dynam*, 44, 279-297.

480 Bosmans, J.H.C., Drijfhout, S., Tuenter, E., Hilgen, F.J., Lourens, L.J. and Rohling, E.J., 2015.
481 Precession and obliquity forcing of the freshwater budget over the Mediterranean. *Quat Sci Rev*,
482 123, 16-30.

483 Bryden, H.L. and Stommel H.M., 1984. Limiting processes that determine basic features of the
484 circulation in the Mediterranean Sea. *Oceanol Acta*, 7, 289-296.

485 Cacho, I., Grimalt, J.O., Canals, M., Sbaifi, L., Shackleton, N., Schonfeld, J. and Zahn, R., 2001.
486 Variability of the western Mediterranean Sea surface temperature during the last 25 000 years
487 and its connection with the northern hemisphere climatic changes. *Paleoceanography*, 16, 40-52.

488 Cacho, I., Sierro, F., Shackleton, N.J., Elderfield, H. and Grimalt, J., 2002. Reconstructing
489 Alboran Sea hydrography during the last organic rich layer formation. *Geochim Cosmochim Acta*,
490 66 (A115).

491 Calvert, S.E. and Pedersen, T.F., 2007. Elemental proxies for palaeoclimatic and
492 palaeoceanographic variability in marine sediments: interpretation and application. In: Hillaire-

493 Marcel, C., Vernal, A.D. (Eds.), *Proxies in Late Cenozoic Paleoceanography*. Elsevier,
494 Amsterdam.

495 Chase Z., Anderson R.F. and Fleisher M.Q., 2001. Evidence from authigenic uranium for
496 increased productivity of the glacial subantarctic ocean. *Paleoceanography*, 16, 468-478.

497 Comas, M.C. and Ivanov, M.K., 2006. Eastern Alboran margin: the transition between the
498 Alboran and the Balearic-Algerian basins. In: Kenyon, H., Ivanov, M.K., Akhmetzhanov, A.M.,
499 Kozlova, E.V. (Eds.) *Interdisciplinary geoscience studies of the Gulf of Cadiz and Western*
500 *Mediterranean basins*; IOC Technical Series. UNESCO, pp. 48-55.

501 Cramp, A. and O'Sullivan, G., 1999. Neogene sapropels in the Mediterranean: A review. *Mar*
502 *Geol*, 153, 11-28, doi:10.1016/S0025-3227(98)00092-9.

503 De Lange, G.J., Thomson, J., Reitz, A., Slomp, C.P., Principato, M.S., Erba, E. and Corselli, C.,
504 2008. Synchronous basin-wide formation and redox-controlled preservation of a Mediterranean
505 sapropel. *Nature Geosci*, 1, 606-610.

506 Dymond, J., Suess, E. and Lyle, J.M., 1992. Barium in deep-sea sediment: A geochemical proxy
507 for paleoproductivity. *Paleoceanograph*, 7, 163-181, doi:10.1029/92PA00181.

508 Eagle, M., Paytan, A., Arrigo, K., Van Dijken, G. and Murray, R. 2003. A comparison between
509 excess Barium and Barite as indicators of export production. *Paleoceanograph*, 18, 1021,
510 doi:10.1029/2002PA000793.

511 Ehrmann, W.U., Schmiedl, G., Hamann, Y., Kuhnt, T., Hemleben, C. and Siebel, W., 2007. Clay
512 minerals in late glacial and Holocene sediments of the northern and southern Aegean
513 Sea. *Palaeogeogr Palaeoclimatol*, 249(1-2), 36-57, doi:10.1016/j.palaeo.2007.01.004.

514 Felis, T. and Rimbu, N., 2010. Mediterranean climate variability documented in oxygen isotope
515 records from northern Red Sea corals. A review. *Global Planet Change*, 71, 232-241.

516 Frank, M., Whiteley, N., Kasten, S., Hein, J.R. and O'Nions, R.K., 2002. North Atlantic Deep
517 Water export to the Southern Ocean over the past 14 Myr: Evidence from Nd and Pb isotopes in
518 ferromanganese crusts. *Paleoceanography*, 17, 1022, doi:10.1029/2000PA000606.

519 Frigola, J., Moreno, A., Cacho, I., Canals, M., Sierro, F.J., Flores, J.A., Grimalt, J.O., Hodell,
520 D.A. and Curtis, J.H., 2007. Holocene climate variability in the western Mediterranean region
521 from a deepwater sediment record. *Paleoceanography*, 22, PA2209, doi:10.1029/2006PA001307.

522 Font, J., 1987. The path of the Levantine Intermediate Water to the Alboran Sea. *Deep-Sea Res*,
523 34, 1745-1755.

524 Goldstein, S.L. and Hemming, S.R., 2003. Long-lived Isotopic Tracers in Oceanography,
525 *Paleoceanography and Ice Sheet Dynamics*. In: H. Elderfield (Ed.). *Treatise on Geochemistry*.
526 Elsevier, Oxford, 453-489.

527 Grimm, R., Maier-Reimer, E., Mikolajewicz, U., Schmiedl, G., Müller-Navarra, K., Adloff, F.,
528 Grant, K.M., Ziegler, M., Lourens, L.J. and Emeis K-C., 2015. Late glacial initiation of Holocene
529 eastern Mediterranean sapropel formation. *Nature Geosci*, 6, 7099, doi:10.1038/ncomms8099.

530 Gutjahr, M., Frank, M., Stirling, C.H., Keigwin, L.D. and Halliday, A. N., 2008. Tracing the Nd
531 isotope evolution of north Atlantic deep and intermediate waters in the western north Atlantic
532 since the Last Glacial Maximum from Blake Ridge sediments. *Earth Planet Sci Lett*, 266, 61-77.

533 Hayes, A., Kucera, M., Kallel, N., Sbeffi, L. and Rohling, E.J., 2005. Glacial Mediterranean sea
534 surface temperatures based on planktonic foraminiferal assemblages. *Quat Sci Rev*, 24, 999-1016.

535 Hennekam, R., Jilbert, T., Schnetger, B. and de Lange, G.J., 2014. Solar forcing of Nile discharge
536 and sapropel S1 formation in the early to middle Holocene eastern
537 Mediterranean. *Paleoceanography*, 29, 2013PA002553.

538 Henry, F., Jeandel, C. and Minster, J.F., 1994. Particulate and dissolved Nd in the Western
539 Mediterranean Sea: Sources, fates and budget. *Mar Chem*, 45, 283-305.

540 Hernandez-Molina, F.J., Somoza, L., Vázquez, J.T., Lobo, F., Fernández-Puga, M.C., Llave, E.
541 and Díaz del Río, V., 2002. Quaternary stratigraphic stacking patterns on the continental shelves
542 of the southern Iberian Peninsula: their relationship with global climate and paleoceanographic
543 changes. *Quat Int*, 92, 5-23.

544 Hernandez-Molina, F.J., Stow, D.A.V., Alvarez-Zarikian, C.A., Acton, G., Bahr, A., Balestra, B.,
545 Ducassou, E., Flood, R., Flores, J-A., Furota, S., Grunert, P., Hodell, D., Jimenez-Espejo, F.J.,

546 Kim, J.K., Krissek, L., Kuroda, J., Li, B., Llave, E., Lofi, J., Lourens, L., Miller, M., Nanayama,
547 F., Nishida, N., Richter, C., Roque, C., Pereira, H., Sanchez-Goñi, M.F., Sierro, F.J., Singh, A.D.,
548 Sloss, C., Takashimizu, Y., Tzanova, A., Voelker, A., Williams, T. and Xuan, C., 2014. Onset of
549 Mediterranean outflow into the North Atlantic. *Science*, 344, 1244-1250,
550 doi:10.1126/science.1251306.

551 Ivanovic, R.F., Valdes, P.J., Gregoire, L., Flecker, R. and Gutjahr, M., 2014. Sensitivity of
552 modern climate to the presence, strength and salinity of Mediterranean-Atlantic exchange in a
553 global general circulation model. *Clim Dynam*, 42, 859-877, doi:10.1007/s00382-013-1680-5.

554 Jacobsen, S.B. and Wasserburg, G.J., 1980. Sm/Nd isotopic evolution of chondrites. *Earth Planet*
555 *Sci Lett*, 50, 139-155.

556 Jeandel, C., Aesouze, T., Lacan, F., Téchiné, P. and Dutay, J.-C., 2007. Isotopic Nd
557 compositions and concentrations of the lithogenic inputs into the ocean: A compilation, with an
558 emphasis on the margins. *Chem Geol*, 239, 156-164.

559 Jimenez-Espejo, F.J., Martinez-Ruiz, F., Sakamoto, T., Iijima, K., Gallego-Torres, D. and
560 Harada, N., 2007. Paleoenvironmental changes in the western Mediterranean since the last
561 glacial maximum: high resolution multiproxy record from the Algero-Balearic basin.
562 *Palaeogeogr Palaeoclimatol*, 246, 292-306.

563 Jimenez-Espejo, F.J., Martinez-Ruiz M., Rogerson M., Gonzalez-Donoso J.M., Romero O.E.,
564 Linares D., Sakamoto T., Gallego-Torres D., Rueda-Ruiz J.L., Ortega-Huertas M. and Perez-
565 Claros J.A., 2008. Detrital input, productivity fluctuations, and water mass circulation in the
566 westernmost Mediterranean Sea since the Last Glacial Maximum. *Geochem Geophys Geosyst*, 9,
567 Q11U02, doi:10.1029/2008GC002096.

568 Johnson, R.G., 1997. Climate control requires a dam at the Strait of Gibraltar. *Eos Trans. AGU*,
569 78, 277, 280-281.

570 Lacan, F., Tachikawa, K. and Jeandel, C., 2012. Neodymium isotopic composition of the oceans:
571 A compilation of seawater data. *Chem Geol*, 300-301, 177-194.

572 Llave, E., Hernández-Molina, F.J., Somoza, L., Stow, D.A.V. and Díaz Del Río, V., 2007.
573 Quaternary evolution of the contourite depositional system in the Gulf of Cádiz. *Geol Soc Spec*
574 *Publ*, 276, 49-79, doi:10.1144/GSL.SP.2007.276.01.03.

575 Mangini, A., Jung, M. and Laukenmann, S., 2001. What do we learn from peaks of uranium and
576 of manganese in deep sea sediments? *Mar Geol*, 177, 63-78.

577 Marcott, S.A., Bauska, T.K., Buizert, C., Steig, E.J., Rosen, J.L., Cuffey, K.M., Fudge, T.J.,
578 Severinghaus, J.P., Ahn, J., Kalk, M.L., McConnell, J.R., Sowers, T., Taylor, K.C., White,
579 J.W.C., and Brook, E.J., 2014. Centennial-scale changes in the global carbon cycle during the
580 last deglaciation. *Nature*, 514, 616-619.

581 Martín-Puertas, C., Jiménez-Espejo F.J., Martínez-Ruiz F., Nieto-Moreno V., Rodrigo M., Mata
582 M.P. and Valero-Garcés B.L., 2010. Late Holocene climate variability in the southwestern
583 Mediterranean region: An integrated marine and terrestrial geochemical approach. *Clim Past*, 6,
584 807-816.

585 Martrat, B., Grimalt, J.O., Lopez-Martinez, C., Cacho, I., Sierro, F.J., Flores, J.A., Zahn, R.,
586 Canals, M., Curtis, J.H. and Hodell, D.A., 2004. Abrupt temperature changes in the western
587 Mediterranean over the past 250,000 years. *Science*, 306, 1762-1765.

588 McManus, J.F., Francois R., Gherardi J. -M., Keigwin L.D. and Brown-Leger S., 2004. Collapse
589 and rapid resumption of Atlantic meridional circulation linked to deglacial climate changes.
590 *Nature*, 428, 834-837, doi:10.1038/nature02494.

591 MerMex Group: Durrieu de Madron, X., Guieu, C., Sempéré, R., Conan, P., Cossa, D.,
592 D'Ortenzio, F., Estournel, C., Gazeau, F., Rabouille, C., Stemmann, L., Bonnet, S., Diaz, F.,
593 Koubbi, P., Radakovitch, O., Babin, M., Baklouti, M., Bancon-Montigny, C., Belviso, S.,
594 Bensoussan, N., Bonsang, B., Bouloubassi, I., Brunet, C., Cadiou, J.-F., Carlotti, F., Chami, M.,
595 Charmasson, S., Charrière, B., Dachs, J., Doxaran, D., Dutay, J.-C. and Elbaz-Poulichet, F., 2011.
596 Marine ecosystems' responses to climatic and anthropogenic forcings in the Mediterranean. *Prog*
597 *Oceanograp*, 91, 97-166.

598 Millot, C.J., 1999. Circulation in the western Mediterranean Sea. *Mar Syst*, 20, 423-442,
599 doi:10.1016/S0924-7963(98).00078-5.

600 Millot, C.J., 2009. Another description of the Mediterranean Sea outflow. *Prog Oceanogr*, 82,
601 101-124, doi:10.1016/j.pocean.2009.04.016.

602 Millot, C.J., 2014. Heterogeneities of in-and out-flows in the Mediterranean Sea. *Prog Oceanogr*,
603 120, 254-278, doi:10.1016/j.pocean.2013.09.007.

604 Moreno, A., Cacho, I., Canals, M., Grimalt, J.O., Sanchez-Goñi, M.F., Shackleton, N. and Sierro,
605 F.J., 2005. Links between marine and atmospheric processes oscillating on a millennial time-
606 scale. A multi-proxy study of the last 50,000 yr from the Alboran Sea (Western Mediterranean
607 Sea). *Quat Sci Rev*, 24, 1623-1636.

608 Naranjo, C., García-Lafuente J., Sánchez-Garrido J.C., Sánchez-Román A. and Delgado-Cabello
609 J., 2012. The Western Alboran Gyre helps ventilate the Western Mediterranean Deep Water
610 through Gibraltar. *Deep-Sea Res PT I*, 63, 157-163. doi:10.1016/j.dsr.2011.10.003.

611 Nieto-Moreno, V., Martinez-Ruiz, F., Willmott, V., García-Orellana, J., Masque, P. and
612 Sinninghe-Damste, J.S., 2013. Climate conditions in the westernmost Mediterranean over the last
613 two millennia: an integrated biomarker approach. *Org Geochem*, 55, 1-10, doi:
614 10.1016/j.orggeochem.2012.11.001.

615 Ovchinnikov, I.M., Plakhin A., Moskalenko L.V., Neglyad K.V., Osadchiy A.S., Fedoseyev A.F.,
616 Krivoscheya V.G. and Voytova K.V., 1976. *Hydrology of the Mediterranean Sea*.
617 Gidrometeoizdat, Leningrad. 375 pp.

618 Palomino, D., Vázquez, J.-T., Ercilla, G., Alonso, B., López-González, N. and Díaz-del-Río, V.,
619 2011. Interaction between seabed morphology and water masses around the seamounts on the
620 Motril Marginal Plateau (Alboran Sea, Western Mediterranean). *Geo-Mar Lett*, 31, 465-479.

621 Parrilla, G., Kinder, T.H. and Preller, R.H., 1986. Deep and intermediate Mediterranean water in
622 the western Alboran Sea. *Deep-Sea Res PT I*, 33, 55-88.

623 Pin, C. and Zalduegui, J.S., 1997. Sequential separation of light rare-earth elements, thorium and
624 uranium by miniaturized extraction chromatography: application to isotopic analyses of silicate
625 rocks. *Anal Chim Acta*, 339, 79-89.

626 Rimbu, N., Lohmann G., Lorenz S.J., Kim J.H. and Schneider R.R., 2004. Holocene climate
627 variability as derived from alkenone sea surface temperature and coupled ocean-atmosphere
628 model experiments. *Clim Dynam*, 23, 215–227, doi:10.1007/s00382-004-0435-8.

629 Roberts, N., Jones M.D., Benkaddour A., Eastwood W.J., Filippi M.L., Frogley M.R., Lamb H.F.,
630 Leng M.J., Reed J.M., Stein M., Stevens L., Valero-Garcés B. and Zanchetta G., 2008. Stable
631 isotope records of Late Quaternary climate and hydrology from Mediterranean lakes: The
632 ISOMED synthesis. *Quat Sci Rev*, 27(25–26), 2426–2441, doi:10.1016/j.quascirev.2008.09.005.

633 Roberts, N.L., Piotrowski, A.M., McManus, J.F. and Keigwin L.D., 2010. Synchronous deglacial
634 overturning and water mass source changes. *Science*, 327, 75–78.

635 Rogerson, M., Rohling E.J., Weaver P.P.E. and Murray J.W., 2005. Glacial to interglacial
636 changes in the settling depth of the Mediterranean Outflow plume. *Paleoceanography*, 20, PA.
637 3007, doi:10.1029/2004PA001106.

638 Rogerson, M., Rohling E.J. and Weaver P.P.E., 2006. Promotion of meridional overturning by
639 Mediterranean-derived salt during the last deglaciation. *Paleoceanography*, 21, PA. 4101,
640 doi:10.1029/2006PA001306.

641 Rogerson, M., Cacho I., Jimenez-Espejo F.J., Reguera M.I., Sierro F.J., Martinez-Ruiz F.,
642 Frigola J. and Canals M., 2008. A dynamic explanation for the origin of the western
643 Mediterranean organic-rich layers. *Geochem Geophys Geosy*, 9, Q07U01,
644 doi:10.1029/2007GC001936.

645 Rogerson, M., Bigg, G.R., Rohling, E.J. and Ramirez, J., 2012a. Vertical density gradient in the
646 eastern North Atlantic during the last 30,000 years. *Clim Dynam*, 39, 589–598.

647 Rogerson, M., Rohling, E.J., Bigg, G.R. and Ramirez, J., 2012b. Paleocyanography of the
648 Atlantic-Mediterranean exchange: Overview and first quantitative assessment of climatic forcing.
649 *Rev Geophys*, 50, RG2003, doi: 10.1029/2011rg000376.

650 Rohling, E.J. and Bryden, H.L., 1992. Man-induced salinity and temperature increases in western
651 Mediterranean deep water. *J Geophys Res*, 97, doi: 10.1029/92JC00767.

652 Rohling, E.J., 1994. Review and new aspects concerning the formation of Mediterranean
653 sapropels. *Mar Geol*, 122, 1-28.

654 Rohling, E.J., Marino, G. and Grant, K.M., 2015. Mediterranean climate and oceanography, and
655 the periodic development of anoxic events (sapropels). *Earth Sci Rev*, 143, 62-97.
656 <http://dx.doi.org/10.1016/j.earscirev.2015.01.008>.

657 Rossignol-Strick, M., Nesteroff, W., Olive, P. and Vergnaud-Grazzini, C., 1982. After the
658 deluge: Mediterranean stagnation and sapropel formation. *Nature*, 295, 105-110.

659 Rutberg, R.L., Hemming S.R. and Goldstein S.L., 2000. Reduced North Atlantic Deep Water
660 flux to the glacial Southern Ocean inferred from neodymium isotope ratios. *Nature*, 405, 935-938.

661 Sanchez-Vidal, A., Collier, R.W., Calafat, A., Fabres, J. and Canals, M., 2005. Particulate barium
662 fluxes on the continental margin: A study from the Alboran Sea (Western Mediterranean). *Mar*
663 *Chem*, 93, 105-117, doi:10.1016/j.marchem.2004.07.004.

664 Siirro, F.J., Hodell, D.A., Curtis, J.H., Flores, J.A., Reguera, I., Colmenero-Hidalgo, E., Bárcena,
665 M.A., Grimalt, J.O., Cacho, I., Frigola, J. and Canals, M., 2005. Impact of iceberg melting on
666 Mediterranean thermohaline circulation during Heinrich events. *Paleoceanography*, 20, PA. 2019,
667 doi:10.1029/2004PA001051.

668 Skliris, N., Sofianos, S. and Lascaratos, A., 2007. Hydrological changes in the Mediterranean
669 Sea in relation to changes in the freshwater budget: a numerical modelling study. *J Marine Syst*,
670 65, 400-416, doi:10.1016/j.jmarsys.2006.01.015.

671 Spivack, A.J. and Wasserburg, G.J., 1988. Neodymium isotopic composition of the
672 Mediterranean outflow and the eastern North Atlantic. *Geochim Cosmochim Acta*, 52, 2762-2773.

673 Sprovieri, M., Di Stefano, E., Incarbona, A., Salvaggio Manta, D., Pelosi, N., Ribera d'Alcala, M.
674 and Sprovieri, R., 2012. Centennial- to millennial-scale climate oscillations in the Central-
675 Eastern Mediterranean Sea between 20,000 and 70,000 years ago: evidence from a high-
676 resolution geochemical and micropaleontological record. *Quat Sci Rev*, 46, 126-135,
677 doi:10.1016/j.quascirev.2012.05.005.

678 Stumpf, R., Frank, M., Schönfeld, J. and Haley, B.A., 2010. Late Quaternary variability of
679 Mediterranean Outflow Water from radiogenic Nd and Pb isotopes. *Quat Sci Rev*, 29 (19-20),
680 2462-2472, doi:10.1016/j.quascirev.2010.06.021.

681 Tachikawa, K., Athias, V. and Jeandel, C., 2003. Neodymium budget in the modern ocean and
682 paleoceanographic implications. *J Geophys Res: Oceans*, (1978-2012), 108, 3254. DOI:
683 10.1029/1999JC000285

684 Tachikawa, K., Roy-Barman, M., Michard, A., Thouron, D., Yeghicheyan, D. and Jeandel, C.,
685 2004. Neodymium isotopes in the Mediterranean Sea: comparison between seawater and
686 sediment signals. *Geochim Cosmochim Acta*, 68(14), 3095-3106.

687 Tachikawa, K., Vidal, L., Cornuault, M., Garcial, M., Pothin, A., Sonzogni, C., Bard, E., Menot,
688 G. and Revel, M., 2015. Eastern Mediterranean Sea circulation inferred from the conditions of
689 S1 sapropel deposition. *Clim Past*, 11, 855–867, doi:10.5194/cp-11-855-2015.

690 Tanaka, T., Togashi, S., Kamioka, H., Amakawa, H., Kagami, H., Hamamoto, T., Yuhara, M.,
691 Orihashi, Y., Yoneda, S., Shimizu, H., Kunimaru, T., Takahashi, K., Yanagi, T., Nakano, T.,
692 Fujimaki, H., Shinjo, R., Asahara, Y., Tanimizu, M. and Dragusanu, C., 2000. JNdi-1: a
693 neodymium isotopic reference in consistency with La Jolla neodymium. *Chem Geol*, 168, 279-
694 281.

695 Tribouvillard, N., Algeo, T.J., Lyons, T. and Riboulleau, A., 2006. Trace metals as paleoredox
696 and paleoproductivity proxies: An update. *Chem Geol*, 232, 12-32,
697 doi.org/10.1016/j.chemgeo.2006.02.012.

698 Tolosa, I., Leblond, N., Copin-Montaigut, C., Marty, J.-C., de Mora, S. and Prieur, L.,
699 2003. Distribution of sterol and fatty alcohol biomarkers in particulate matter from the frontal
700 structure of the Alboran Sea (S.W. Mediterranean Sea). *Mar Chem*, 82, 161-183.

701 Toucanne, S., Jouet, G., Ducassou, E., Bassetti, M.-A., Dennielou, B., Minto'o, C.M.A., Lahmi,
702 M., Touyet, N., Charlier, K., Lericolais, G. and Mulder, T., 2012. A 130,000-year record of
703 Levantine Intermediate Water flow variability in the Corsica Trough, western Mediterranean Sea.
704 *Quat Sci Rev*, 33, 55-73. doi:10.1016/j.quascirev.2011.11.020

- 705 Touchan, R., Anchukaitis, K.J., Meko, D.M., Sabir, M., Attalah, S. and Aloui, A.,
706 2010.Spatiotemporal drought variability in northwestern Africa over the last nine centuries. *Clim*
707 *Dynam*, doi:10.1007/s00382-010-0804-4.
- 708 Van der Weijden C.H., 2002. Pitfalls of normalization of marine geochemical data using a
709 common divisor.*Mar Geol*, 184, 167-187.
- 710 Vance, D., Scrivner, A.E., Beney, P., Staubwasser, M., Henderson, G.M. and Slowey, N.C.,
711 2004.The use of foraminifera as a record of the past neodymium isotope composition of seawater.
712 *Paleoceanography*, 19, PA2009, doi: 10.1029/2003PA000957.
- 713 Voelker, A.H.L., Lebreiro, S.M., Schönfeld, J., Cacho I., Erlenkeuser, H. and Abrantes, F., 2006.
714 Mediterranean outflow strengthening during northern hemisphere coolings: A salt source for the
715 glacial Atlantic? *Earth Planet Sci Lett*, 245, 39-55.

Figure 1

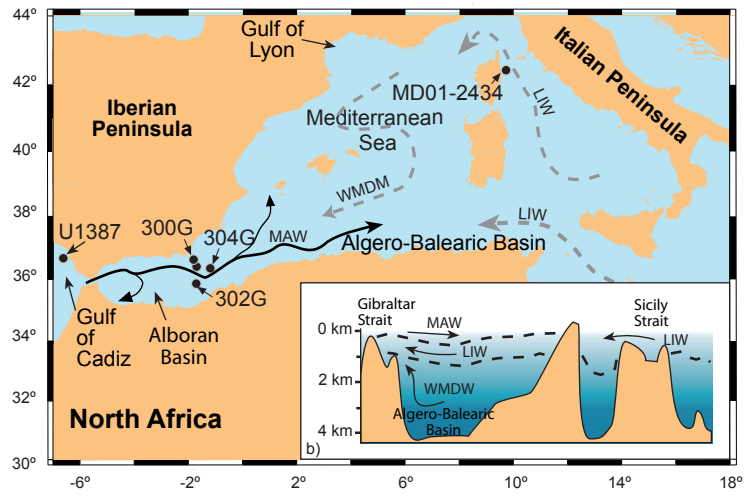


Figure 2

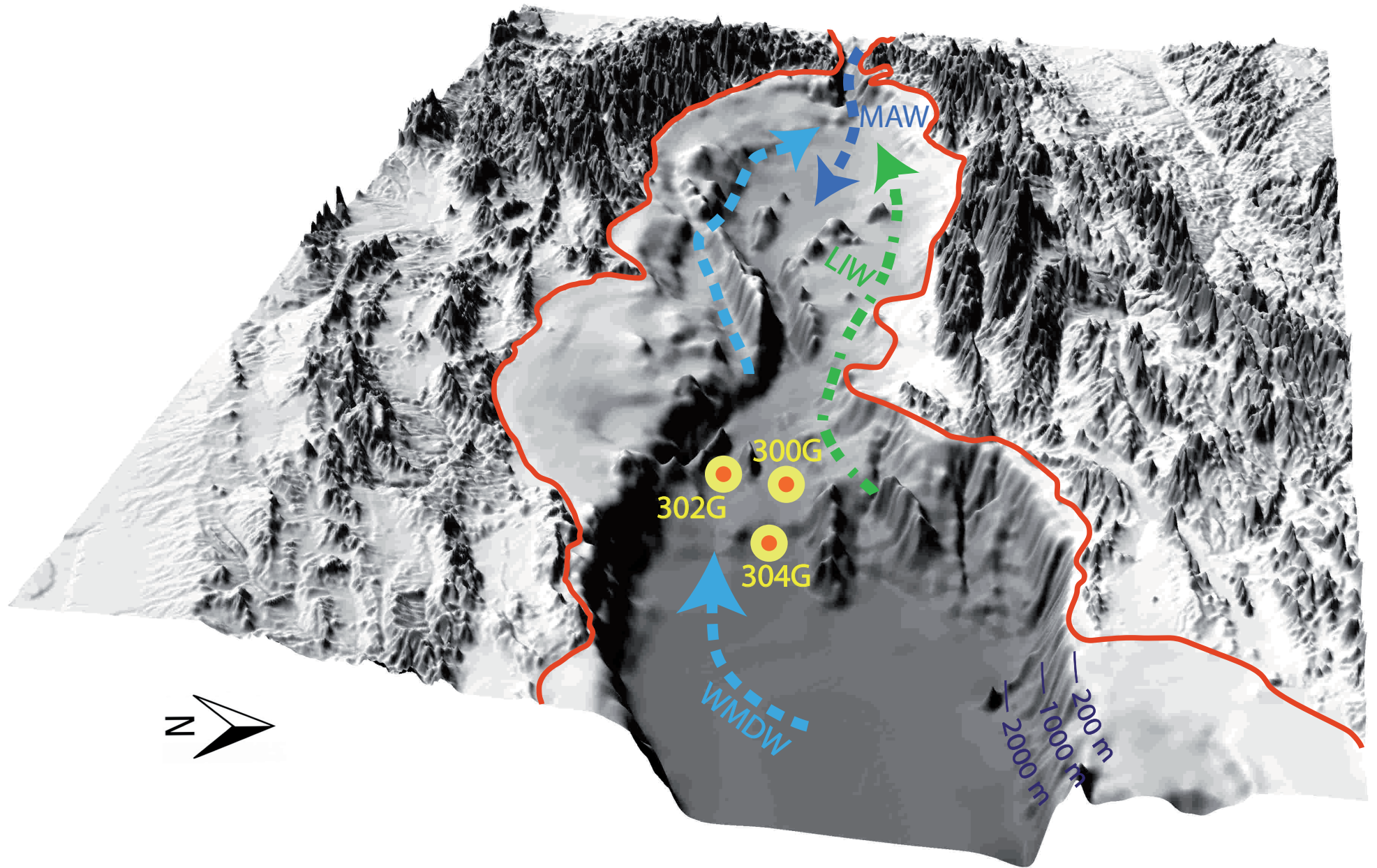
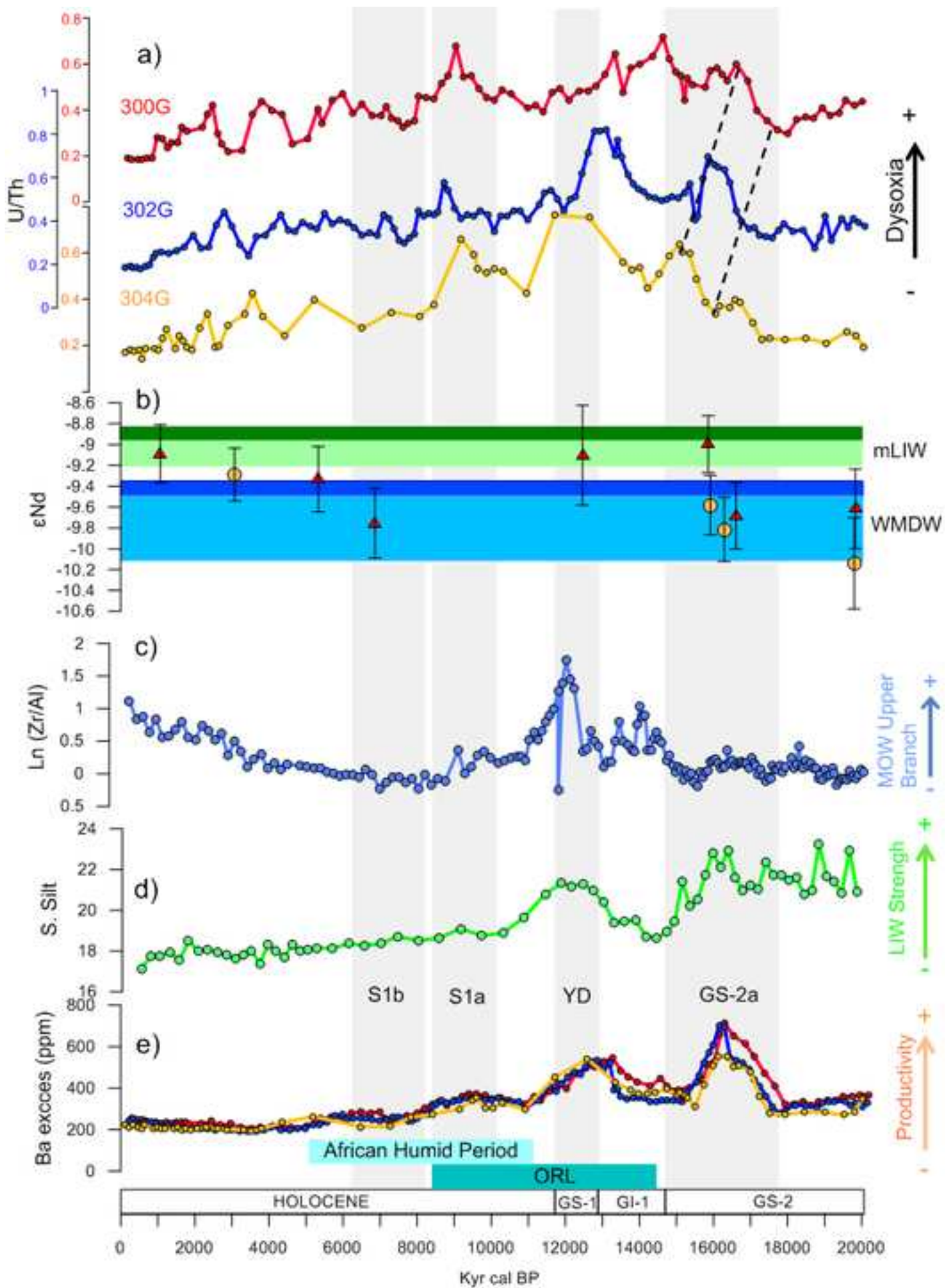


Figure 3
[Click here to download high resolution image](#)



Data set Figure 3

[Click here to download Supplementary Material for on-line publication only: Figure 3 data set.xlsx](#)